

Evaluating Interior Orientation Estimability in Multimedia Photogrammetry - A practical guide on object-invariant bundles

Robin Rofallski¹, Amandine Colson^{2,3}, Thomas Luhmann¹

¹ Institute for Applied Photogrammetry and Geoinformatics, Jade University of Applied Sciences, Oldenburg, Germany
(robin.rofallski, thomas.luhmann)@jade-hs.de

² Denkmal3D, Vechta, Germany - a.colson@denkmal3.de

³ German Maritime Museum, Leibniz Institute for Maritime History, Bremerhaven, Germany

Keywords: Camera Calibration, Multimedia Photogrammetry, Bundle Adjustment, Parameter Estimation, Correlation

Abstract

Bundle adjustment in multimedia environments, such as underwater or through refractive interfaces, poses unique challenges for parameter estimation due to increased correlations between interior orientation and refractive parameters. This contribution investigates the estimability and correlation of these parameters in object-invariant multimedia bundles by presenting both a simulated and a real-world dataset. Using a strict ray tracing bundle adjustment approach, we analyze how water depth, surface tilt, and parameter set selection influence correlations and numerical stability. Statistical metrics - including correlation matrices, parameter significance tests, and variance inflation factors (VIF) - are evaluated for their effectiveness in diagnosing problematic configurations. Results show that while traditional metrics like σ_0 may not reveal instability, VIF and correlation analysis provide practical additional procedures for identifying robust parameter estimations. The findings offer a workflow for practitioners, highlighting optimal parameter configurations and the limitations of statistical diagnostics in multimedia photogrammetry.

1. Introduction

Photogrammetric analysis in and through water becomes increasingly important for the use of natural resources, investigation of marine life and various industrial purposes. For many applications highest accuracy is of utmost importance while avoidable inaccuracies and mistakes should be avoided, regardless of the application. Generally, a substantial accuracy improvement can result from strict modeling of the imaging geometry by including refraction in the bundle adjustment.

Ray tracing is a strict procedure for bundle adjustment to obtain 3D and calibration data from photogrammetric measurements (Mulsow, 2010). However, adjusting both interior orientation parameters (IOP) and refractive parameters can cause high correlations, influenced by the parameter set and bundle configuration. These correlations often lead to substantial errors and cannot be observed directly by the reprojection error (σ_0) or other standard metrics. Evaluating correlation coefficients can help identifying problematic datasets, but correlations may be distributed across the dataset, making it difficult for non-experts to assess result quality. The goal of this contribution is to determine an optimum parameter configuration for an object-invariant bundle where an automated camera system faces through the water surface into a conservation tank. Variance Inflation Factors (VIF) are used to estimate numerical stability from covariance information, not requiring ground truth data.

This paper outlines as follows: After introduction and related work, the methodology for the evaluated object-invariant datasets is presented. Next, two datasets are evaluated with different focuses. First, a simulated semi-spherical bundle is presented and correlations over different parameter changes investigated. Following up is an investigation into a real-world dataset from a monitoring system. The reader is guided

along a practical statistical investigation on the assessment and statistical implications of an exemplary data set with a ray tracing approach. Findings are then discussed, concluded and an outlook on further analyses is given.

2. Related Work

Research on parameter estimability and correlations in photogrammetric bundle adjustment has evolved and is well-understood in air. Investigating and understanding correlations is essential to bundle adjustment in order to estimate 3D coordinates and other parameters accurately and reliably. Luhmann et al. (2020) presents fundamental insights into parameter interactions and correlations between IOP in the Brown model, emphasizing the challenges in decoupling these parameters. A practical guideline is presented on expectable correlations and values are generally classified. Hastedt et al. (2021) thoroughly investigated correlations and adjustments for aspherical cameras to reduce systematic patterns. In this study, the authors also deeply focus on the occurring correlations, especially in an additional calibration model, applying Fourier terms. However, both references do not focus on the special implications in multimedia photogrammetry.

Maas (2015) provided insights on the accuracy potential in underwater photogrammetry and discussed affecting parameters. This includes network geometry, the refractive objects just as physical effects, e.g. dispersion, chromatic aberrations and other image degrading effects. The author states a general accuracy reduction by a factor of 2-5 under favorable laboratory conditions, compared to in-air measurements. Kahmen et al. (2019) focused on multimedia errors, resulting in stereo datasets from neglecting strict modeling, e.g. by implicit calibration. It was found that exterior orientation parameters are correlated with the baseline of stereo partners, affecting the general bundle scale if no other scale representation is present.

Extending this contribution, the authors performed further extensive simulations in Kahmen et al. (2020). The influence of varying acquisition distances was addressed when neglecting refraction for stereo systems. Part of the investigations were analyses on correlation parameters between interior orientation and exterior orientation with respect to different convergence angles of a stereo system, different amounts of water in the ray path just as different object geometries. It was concluded that with higher convergence angles, some correlations disappear, probably favoring these for neglecting strict ray modeling under water. Furthermore, no apparent correlation changes were found when the amount of water in the ray path was changed. Shortis (2019) extensively summarizes approaches to camera calibration in underwater settings. This also includes factors of accuracy and approaches to mitigating accuracy-reducing effects. Among them, the author states best practice approaches for optimum network geometry to reduce correlations, especially when absorbing refraction by implicit calibration. It is stated that a spatial test field, frame-filling acquisition, just as rotation variation, are key to optimum geometries with low correlations. This, of course, holds true not just for underwater settings. Still, an accuracy loss of factor 3-10 from in-air measurements was observed from cited literature. The suggestions were taken up and employed in the simulations of this contribution to provide an optimum network geometry for clear results. Further deeper insights into accuracy evaluations on multimedia datasets are provided by many works of Erica Nocerino and Fabio Menna, e.g. in Nocerino et al. (2018) or Menna et al. (2017).

This contribution focuses on further understanding correlation and parameter estimability in multimedia environments, especially for object-invariant interfaces. It aims to link the guidelines from Luhmann et al. (2020) to multimedia datasets.

3. Adjustment and methodology

3.1 Ray tracing bundle adjustment

For all analyses in this contribution, we used the approach by Rofallski and Luhmann (2022), applied to object-invariant interfaces in Rofallski et al. (2024). It follows the strict mathematics of Snell's law and ray tracing bundle adjustment. The optimization is however transferred from image space to object space, enabling direct computation of the 3D error

function and omitting additional inner loops for computing the ray tracing from point to image. The shifted optimization to object space provides advantages in speed and reliability and is therefore chosen over other implementations. However, findings should be generally transferable to other strict multimedia approaches like the ones from Mulsow (2010) or Kotowski (1987).

Apart from the standard Brown parameters, the refractive parameters included to the bundle are for the water plane in Hesse Normal form with $N = (n_x, n_y, n_z)^T$ and d as absolute value, yielding $\vec{N} \cdot \vec{P}_0 - d = 0$, subject to $\|\vec{N}\| = 1$. μ_w is the refractive index of water and adjusted for while the refractive index of air is held constant $\mu_{air} = 1.00028$. For further details on the approach and ray tracing bundle adjustment, refer to the aforementioned publications.

3.2 Methodology

In the following, two setups are investigated. The first is a pure simulation designed to understand the mechanics of correlations. A spatial test artifact with a semi-spherical arrangement of exterior orientations above provides near-optimal conditions to analyze inevitable correlations in multimedia photogrammetry with object-invariant water surfaces. The second is a real-world example from a wood-monitoring system over a conservation tank, used to assess statistical metrics. To investigate parameter estimability and correlations, six parameter sets were analyzed. Generally, all parameters of exterior orientation (EOP), object points (OP), and refractive parameters (n_x , n_y , d , and implicitly $n_z = \sqrt{1 - n_x^2 - n_y^2}$), denoted "Ref", were adjusted. Pre-calibration was included, either simulated or from the real dataset. For each dataset, interior orientation parameters, namely camera constant (c), principal point (pp), radial symmetric distortion with three parameters (rad), decentering distortion with two parameters (dec), and affinity and shear (aff) were gradually added following definitions from Brown (1971) and El-Hakim (1986).

The simulation focuses on correlations to extend knowledge from air-based studies such as Luhmann et al. (2020) and Hastedt et al. (2021). This is then extended to a best-practice guide for assessing the monitoring system dataset, incorporating additional statistical parameters from literature to estimate photogrammetric multimedia bundle quality.

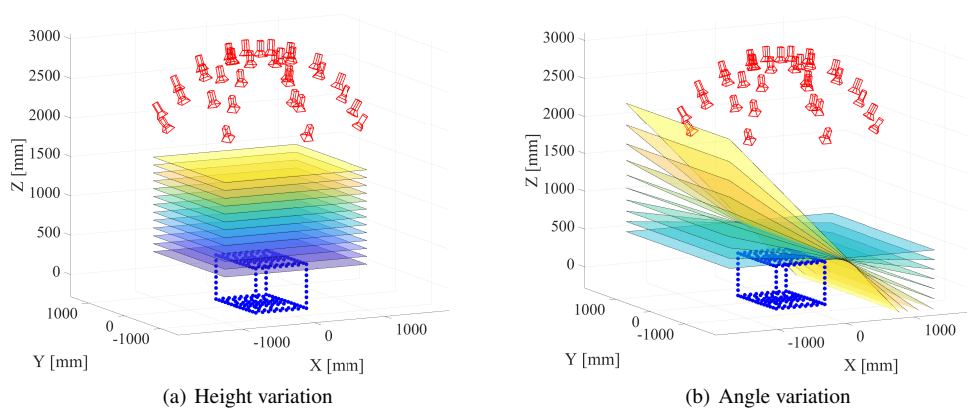


Figure 1. Bundle geometry with respective variation of the water surface by (a) shifting its height along the global Z-axis and tilting it around the X-axis (b). Camera stations are red, object points of spatial test artifact are blue.

4. Simulated datasets

To analyze parameter correlations in multimedia environments, we simulated configurations using a spatial test artifact with semi-spherical bundle geometry. This near-optimal setup (132 cameras arranged spherically at 1500 mm radius/height above a 1000 mm × 700 mm × 500 mm artifact) ensures clear observation of correlation patterns under varying water conditions. We tested water depth variations of 300 - 1500 mm and surface tilts of 45 - 90° while maintaining constant camera and object positions just as error-free image coordinates. Simulation parameters are presented in Table 1. The parameters were chosen to obtain a full frame coverage of image points and otherwise standard values for refractive parameters.

Figure 1 show the bundle geometry with the respective water plane variations for the single simulations. We simulated both an increase of water depth in steps of 100 mm and a tilt of the water surface from fully perpendicular (i.e. 90°) to 45° at a constant water height of 500 mm from the barycenter of the object points. The exterior orientations and locations of the object points remained constant throughout the simulations. Image coordinates were simulated without any errors.

Generally, all adjustments converged to a plausible and accurate solution. The differences in the calibration and in object space were marginal and are not discussed any further here. More interesting were the implications of correlations that arise from this rather favorable bundle geometry. Elements $r_{i,j}$, denoting the correlation coefficient between the i-th and j-th parameter of the adjustment are calculated as follows:

$$r_{i,j} = \frac{\Sigma_{xx_{i,j}}}{\sqrt{\Sigma_{xx_{i,i}} \cdot \Sigma_{xx_{j,j}}} \quad (1)$$

where Σ_{xx} is the covariance matrix of the adjustment.

Figure 2 provides an exemplary correlation matrix from 900 mm water height with all parameters included for adjustment. This is indicative of the increased correlations that we could observe in other datasets from the simulation. Clearly, the functionally known correlations from the standard Brown model were visible, as well. This includes especially the correlations among the radial-symmetric parameters and decentering distortion with the principal point. However, additional correlations, dependent on the imaging geometry occurred and change with different water surface arrangements. Especially, correlation between camera constant and refractive parameters d and μ_w and between d and μ_w show observable trends which are discussed in the following. For the sake of conciseness, we do not present all correlation matrices.

Table 1. Setup parameters for simulated data set

Camera constant c	-20 mm
Principal point	$x'_0 = y'_0 = 0$ mm
Distortion parameters	0
μ_{air}	1.00028
μ_w	1.3318
Image noise	0.0 px
No. cam. stations	132
No. object points	208
No. image points (approx. per bundle)	25,000

4.1 Water height variation

In total, 13 datasets were simulated at water depths of 300 mm to 1500 mm or an air-to-water ratio of 12 % to 58 %. In Agrafiotis and Georgopoulos (2015) and Kahmen et al. (2019), the statistical considerations were related to the air-water ratio, independent of the bundle scale. We also correlate the distances to the water percentage $w\%$ (equal to $100\% - w\%$) to relate our findings to this metric, as well since effects should be transferable to other scales. The values were calculated by the distance between the barycenter of the EOP and the OP and represent an average distance over all coordinates.

In this and the following section, the adjustment with refraction and the camera constant $Ref + c$ is focused as only major correlations and trends between these two parameter sets were found. Furthermore, Figure 3 (a) shows the trend of the three aforementioned correlations of camera constant with refraction parameters and among two of them. Clear trends are observable that show a decline of the two correlations with the refraction index of water μ_w while the correlation between camera constant and the absolute value of the plane (d) rises with increasing water percentage, i.e. a decrease of air-water ratio.

4.2 Tilted water surface

For the tilted dataset, 10 datasets with increments of 5° were simulated. Figure 3 (b) shows the results for the same configuration as a function of the tilting angle of the water surface α . The rotation was carried out around the x-axis which is reflected in correlations between n_x and d just as between n_x and μ_w . Especially these correlations clearly change for different angles (purple and green line). The green curve (n_x, μ_w) exhibits high correlation values close to 1 for smaller angles ($\alpha = 45 - 80^\circ$), indicating a strong linear relationship between these parameters in this range. However, as the angle approaches 90° the correlation rapidly decreases logarithmically, reaching zero at 90°. The same applies to the purple curve (n_x, d), decreasing close to linearly to zero at 90°. This suggests both parameters to be decoupled in this range.

The blue (c, d), red (d, μ_w), and yellow (c, μ_w) curves display intermediate behaviors. The correlation between c and d (blue) slightly increases with α , while the correlation between d and μ_w (red) shows a sinus-like behavior but remaining below 0.8. The correlation between c and μ_w (yellow) remains relatively low and falls to zero at 55° but increases at higher angles. These patterns reflect varying degrees of parameter coupling influenced by the geometric setup.

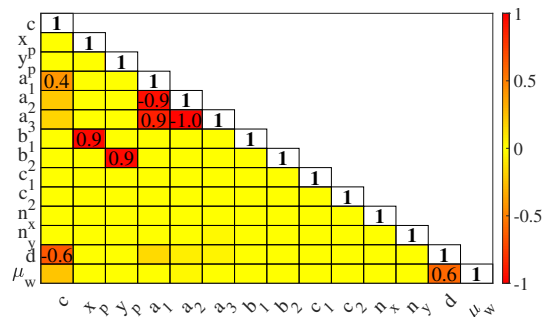


Figure 2. Correlation matrix from dataset with 900 mm, $\alpha = 90^\circ$ water surface and all parameters included

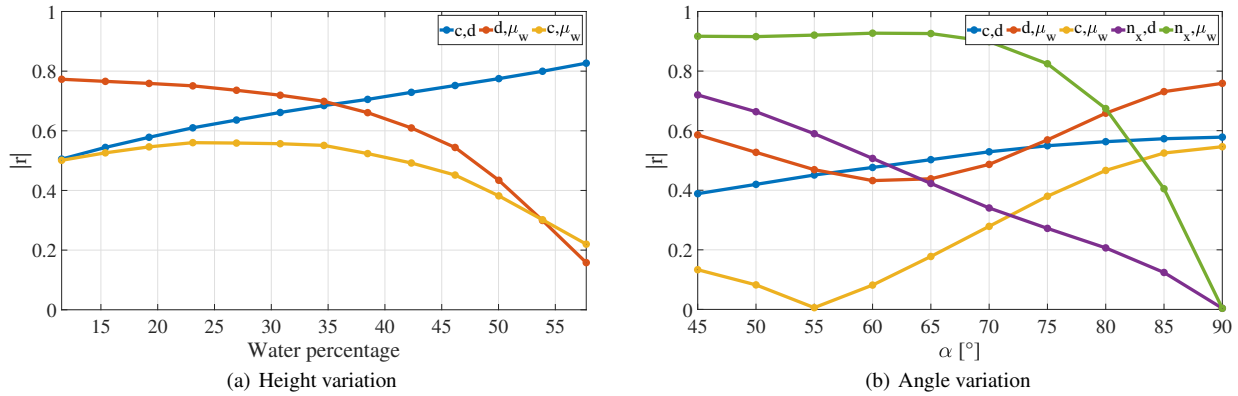


Figure 3. Identified major correlations over the entire simulations for height variation (a) and angle variation (b), $Ref + c$

4.3 Variation between parameter sets

As last investigation, the variation of the major correlation parameters along different parameter sets was examined. From this data, no consistent trends were observable, other than mostly constant tenor. However, as an example, a tilted dataset at 65° is presented as there are all discussed correlations unequal to zero (Figure 4). It is observable that most parameters remained constant over all parameter sets which holds true for the other datasets as well. Some parameters change slightly ($d, \mu_w; c, \mu_w$), starting with the radial-symmetric parameters while these changes are always decreases in correlations. This can be observed from other analyses, as well with different values but remain similar in magnitude.

4.4 Discussion

The three investigations reveal clear trends in five identified major correlations. Correlations with μ_w decreased as more water was added to the ray path, likely because greater water depth allows refraction effects to be better resolved and decouples image scale from this parameter (Nocerino et al., 2021). In contrast, the correlation between c and d increased with higher water percentage, which is expected since shifting the surface toward the camera affects image scale and thus the camera constant, though the exact reason for this increase remains unclear. Angular variation data also showed that the water surface orientation relative to the camera stations influences correlations, particularly as the rotated normal vector component n_x strongly changed its correlation with d and μ_w . This may be because the intersection area between ray paths

and the plane is largest when perpendicular and shrinks at lower angles, reducing the estimability of this rotation. Reducing such correlations, especially near $\alpha = 45^\circ$ may require extra constraints, measurements, or careful experimental design. Whether these correlations impair bundle accuracy depends on the specific dataset and other statistical metrics. In these datasets, all bundles converged correctly without accuracy loss, though this may differ in real-world scenarios with image noise.

Interestingly, the decentering distortion does not show any correlations with the water plane parameters. Since decentering is partly able to absorb the effects of small tilts between camera axis and plane (Shortis, 2019), it would have been expected to show in this dataset, too. This is probably resolved through the full semi-spherical bundle geometry which allows to observe the interface from different angles and distances.

When focusing on the changes in correlations over different parameter sets, it was observable that, apart from a generally non-affected behavior, some correlation parameters, especially c, μ_w decreased when radial-symmetric parameters were added. This is likely due to a "smearing effect" of correlations when additional parameters are introduced, particularly the radially symmetric component, which can partially account for an increased image scale. This would affect both the camera constant c and refraction (d and μ_w).

Simulating down to a mean angle of 45° between the main observation axis and the water surface is rather theoretical, since total internal reflection occurs at $\alpha = \arcsin(n_{air}/n_w) = 48.7^\circ$, so some orientations may not observe all submerged object points. This effect was not considered in the simulation and could influence the continuous correlation trends.

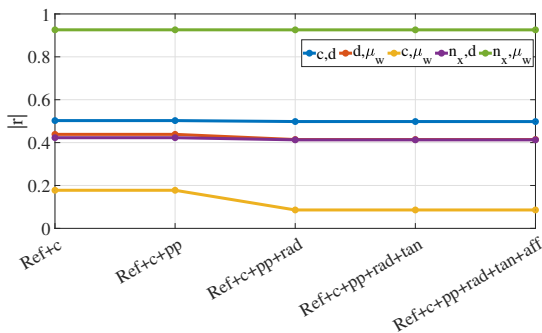
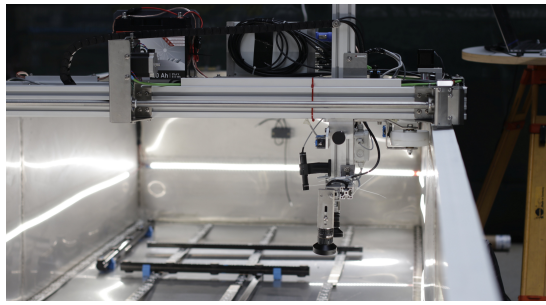


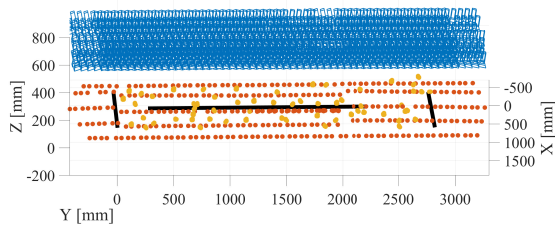
Figure 4. Identified major correlations over the entire simulations for 500 mm water depth and 65° tilting angle

5. Wood monitoring dataset

The investigated setup is based on the developed monitoring system in the DBU-funded project "OptiKons" (Rofallski et al., 2024). It aims to understand and quantify deformations on archaeological wood during conservation treatment. The system consists of a biaxial measurement unit, carrying a stereo camera system on top of a water tank, used for treatment (Fig. 6 (a)). The cameras face downwards through the liquid surface, creating a multimedia photogrammetric problem with refraction at the liquid surface. According to Kotowski (1987), this is an object-invariant setup, meaning that the refractive surface remains stable with respect to the object while the



(a) Biaxial measurement unit



(b) Bundle geometry (Rofallski et al., 2024)

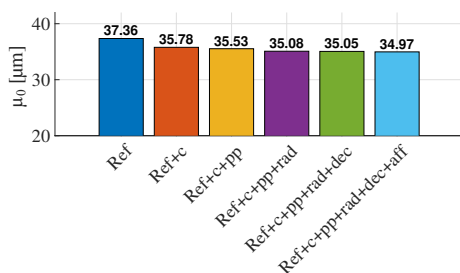
Figure 6. Automated measurement system (top) and resulting bundle geometry (bottom). Camera stations are blue, object points red/orange and scale bars black.

camera moves independent of this setup. The camera system meanders over the object points but does not employ rotation or height variation (Fig. 6 (b)).

In a previous study, the configuration to adjust for EOP, OP, refractive parameters and a free relative orientation between the stereo pairs was deemed to provide the best results (Rofallski et al., 2024). Consistently with the previous section, this setup is referred to as *Ref* with all added parameters being named analogously. For scale definition, a single CFRP scale bar placed in the middle of the bundle with 2 m length was used.

5.1 Best practice for single dataset

To guide readers, this section provides a guideline for possible parameters and statistical values that may provide information about the reliability of a solution when no ground truth is present. These guidelines apply equally to multimedia datasets and to regular single-media or other configurations. The statistical indicators are presented along a representative dataset from the monitoring system. Usually, it is not feasible for a practitioner to obtain ground truth data due to time or practical concerns, especially in refractive environments. However, to better understand the subsequent results, the accuracy estimate



(a) Standard deviation of unit weight

is presented first to observe differences between ground truth and statistical metrics.

LME values To estimate accuracy, two independent, calibrated CFRP scale bars (1 m each) were used. Length measurement errors (LME) were calculated for all parameter sets according to VDI/VDE 2634-1, which defines the maximum error as the decisive metric (VDI/VDE, 2002). Figure 5 (b) shows maximum LME values for all performed adjustments. Values decrease across the first three configurations, reaching a minimum when adjusting refraction, *c*, and *pp*, but increase again with more parameters, partly exceeding the refraction-only case. This independent metric should be considered in the following when evaluating the statistical metrics, as it highlights potential pitfalls of relying solely on statistical parameters.

Standard deviation of unit weight The first evaluation towards data quality usually is performed, using the standard deviation of unit weight after adjustment (σ_0). Figure 5 (a) shows the respective values for each parameter set. These are generally comparable but show the expected trend of decreasing magnitude towards more estimated parameters with the minimum of 34.97 μm for the dataset with all parameters estimated (*Ref+c+pp+rad+dec+raff*). From this analysis, no implication towards an accuracy decline with the last three adjustments can be made.

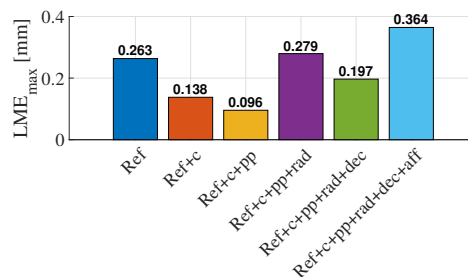
Parameter significance Next, information from the covariance matrix can be used to estimate standard deviations of the estimated parameters.

$$\Sigma_{xx} = \sigma_0^2 \cdot (J^T P J)^{-1} \quad (2)$$

The estimated standard deviation for the *i*-th parameter is calculated from the main diagonal of the covariance matrix:

$$\sigma_{x_i} = \sqrt{\Sigma_{xx_{i,i}}} \quad (3)$$

It is desirable to receive significant parameter results, meaning that the standard deviation of each parameter should be significantly lower than its estimated value. This can be calculated by performing Student's t-test. However, it is not feasible to assess all parameters, including EOP and OP values for they are usually large in numbers and therefore hard to locate single parameters. Figure 7 shows a bar chart of the test statistics for each parameter set from one of the two interior orientations. A practical confidence value of 95 % was chosen, yielding a t-value of 1.96, indicated by the horizontal dashed line. Values above this line are considered significant while



(b) Maximum length measurement errors

Figure 5. Standard deviation of unit weight after adjustment (left) and maximum LME values for the investigated dataset (right). Clearly, the standard deviation does not reflect the independent quality measure of the corresponding LME.

values below that are considered non-significant and may pose a problem in adjustment due to correlation with other parameters. The figure is grouped by the respective parameter and shows the corresponding test statistic:

$$t_i = \frac{x_i}{\sigma_{x_i}} \quad (4)$$

It can be observed that the test statistic decreases for all other values when more unknown parameters are being estimated, i.e. lower redundancy. Furthermore, all values up to $Ref + c + pp + rad$ are above the significance value, implying no further problems or quality decline. Additionally adjusting for decentering distortion and affinity and shear yielded non-significant values which are still close to significance, except for b_2 in the last parameter set. It also becomes apparent that other parameters are affected and reduce their statistic value when distortion terms rad , dec and/or aff are added, most notably with the camera constant. From this data, datasets with dec and aff appear suspicious for harmful correlations.

The test statistic decreases as more parameters are added (reducing redundancy). All adjustments up to $Ref + c + pp + rad$ remain above the significance threshold, indicating reliability. However, adding decentering distortion and affinity/shear yields non-significant values, though being near the threshold, particularly for b_2 . The camera constant shows reduced significance when distortion terms (rad , dec , aff) are included, suggesting harmful correlations in these datasets.

Correlation matrix Thus, the next information that can be derived from the covariance or cofactor matrix is the correlation matrix \mathbf{R} as described in the section before. Analysis of the correlation matrix can be performed globally by assessing the magnitude of the single correlations and their amounts. Also, the matrix can be investigated by assessing single local parameter combinations to identify possibly problematic parameters that are correlated or obsolete. Generally, polynomial parameters are strongly correlated with each other, often reaching values close to 1. This usually is not a problem, as long as the parameters are statistically significant and correlations do not reach $r = 1$. Also, decentering parameters are often correlated with the principal point which is also present in this dataset (Luhmann et al., 2020).

Since $r_{i,j} = r_{j,i}$, \mathbf{R} is a symmetric matrix. Thus, we depict the lower triangular matrix as a heat map in Figure 8 for all six parameter sets. Correlation coefficients $|r| \geq 0.4$ are printed while the other elements are shown true to the color map. Again, only the first camera is depicted to be a representative sample. Results and findings are similar and transferable.

Datasets including refraction, camera constant, and principal point (a-c) exhibit small correlations. Introducing distortion polynomials (d) increases correlations, particularly between refractive parameters, c , and pp . Known functional correlations emerge in sets d-f, with strong links between c and y_p , and between d , y_p , and decentering distortion. While affinity/shear adjustments (f) reduce camera constant correlations, decentering distortion and d remain correlated.

Generally, it is not straight-forward to single out one dataset that contains a number of correlations that should provide the maximum accuracy possible. However, when considering the full adjustment series, it can be concluded that with the inclusion of radial-symmetric parameters and all additional parameters, problematic correlations occur. Contrarily, if only the dataset with all parameters was present, it might not be clear whether that dataset contains problematic correlations.

Variance inflation factors The last metric for this dataset is the Variance Inflation Factor (VIF), a well-known measure from statistics which is not very present in photogrammetry or geodesy (Kutner et al., 2005). VIF is defined as

$$VIF_i = \frac{1}{1 - R^2} \quad (5)$$

with R^2 being the coefficient of determination. VIF is calculated as a ratio between the parameters' variance in the full model with all correlations (multivariate) and a univariate model without correlations. From this transition, it can be shown that VIF can also be calculated from the main diagonals of the normal equation matrix ($\mathbf{N} = \mathbf{J}^T \mathbf{P} \mathbf{J}$) and the cofactor matrix ($\mathbf{Q}_x = \mathbf{N}^{-1}$) (Kutner et al., 2005):

$$VIF_i = N_{i,i} \cdot Q_{x_{i,i}} \quad (6)$$

VIF provides a metric, how well one parameter can be estimated by the other parameters by analyzing the cofactor or

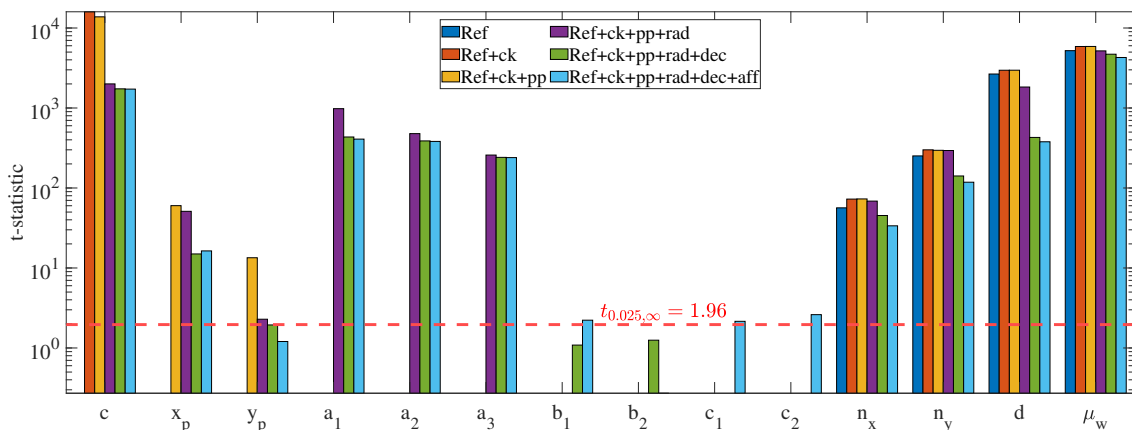


Figure 7. t-statistics for each evaluated parameter set on logarithmic scale. Red dashed line indicates 0.025 percentile (two-sided test) for 95 % confidence at infinite degree of freedom, i.e. normal distribution.

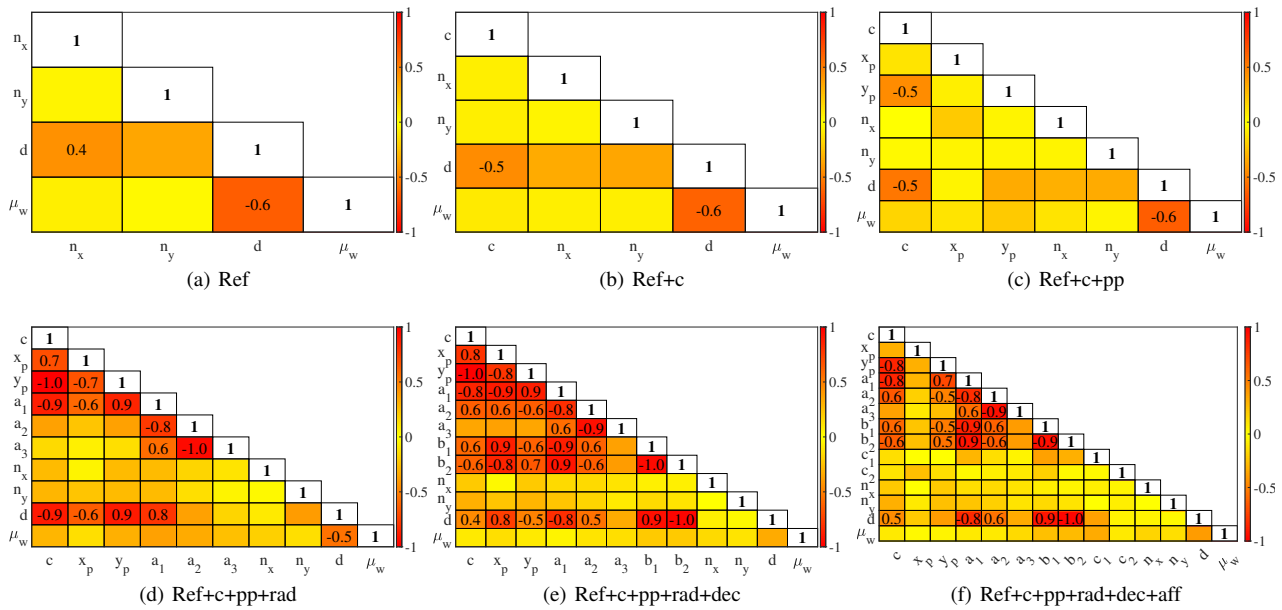


Figure 8. Correlation coefficients for different analyses. Only values $|r| \geq 0.4$ are printed out.

covariance matrix. Generally, $VIF \geq 10$ for a given parameter implicate possibly problematic correlations between parameters that may have degrading effects on the numerical stability of least squares adjustment. Conversely, very small or large values often indicate poor matrix conditioning, potentially due to an unstable adjustment (Kutner et al., 2005). These factors, computed per variable, reflect the inflation from an uncorrelated to a correlated adjustment.

Figure 9 shows a heatmap of the adjusted parameter sets on the x-axis and the respective parameters on the y-axis. The VIF values are color coded, according to the guidelines presented. From the figure, the key insights are that all values for adjustments without polynomial parameters are below 5 and hence implicate statistical reliability. From there, especially the radial and decentering parameters show to be strongly affected, just as the camera constant and the d value from the water plane. However, values are directly associated with a distinct value which can be interpreted and compared against a threshold.

5.2 Discussion

The data with the lowest LME values result from the adjustment including refraction, camera constant and principal point. These parameters are rather simple in its mathematical form (contrary to polynomial parameters a, b, c) and therefore usually easier to estimate. However, especially due to the missing rotation and height variation, it was not necessarily anticipated to return better results. The original calibration took place about four months prior to the dataset. Analyzing the values for the camera constant and principal point, two distinct changes were observable. For one, y_p increased whereas x_p remained identical within statistical error margins. Additionally, the camera constant increased slightly. This could indicate a tilt of the lens, leveraging on the mount. Since the cameras were oriented oblique, gravity acting on the lens mount could provoke this behavior. It appears consistent with the fact that the pre-calibration was performed outside the water tank with the cameras facing in a horizontal direction. This could have introduced small changes on the positioning. Furthermore,

temperature and humidity on site were not controlled and hence might have impacted the values further over time.

The presented statistical parameters provide a guideline for a user to understand the quality of the acquired data. In the presented case, not all of these parameters pointed towards the parameter set with the lowest LME. It can especially be concluded that the standard deviation of unit weight cannot point towards the best solution in this case. However, if no systematic errors or major correlations are present, this metric can work as an accuracy estimate. In this case, the t-test on parameter significance pointed out that the adjustments

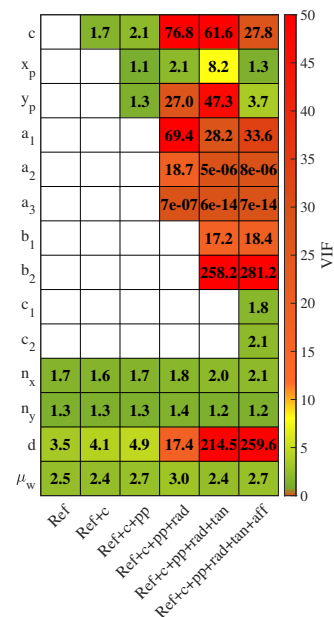


Figure 9. Variance inflation factors for evaluated parameter sets. Evaluated parameter sets are on the horizontal axis, parameters are on the vertical axis. Values below 1 and over 10 are red, gradually turning yellow and green in between.

with decentering and affinity/shear could be problematic but it failed to show clear tendencies towards the radial parameters. From the correlation analysis, it became more clear that also the radial parameters affect the solution and VIF additionally attributed a number to that tendency. While the findings from the correlation analysis back these values, the correlation matrices do not show the implications per parameter but only per parameter pair. Here, it can clearly be stated where a starting point for optimization could be. Employing VIF in practical adjustments can be done similarly to a Baarda test by removing the parameter (block) with the highest VIF and then re-running the adjustment until all values are below the threshold of 10. The observed strong correlations between refractive parameter d and the decentering distortion may most likely arise due to the missing rotation around the optical axis. Hence, decentering can probably explain most of the refractive plane which is not resolved by different rotations.

6. Conclusion

With this contribution, insights on the behavior of correlations and estimability of parameters for object-invariant multimedia bundles were presented. Along with theoretical investigations on a simulated dataset, a real-world example was presented and practically investigated. It is hard to generalize the findings and transfer them completely to other data, as this dataset is only a very limited sample. Other geometries, applications or configurations may yield different results which may have to be treated differently. Therefore, it is always advisable to look through all possible statistical metrics and/or - if possible - acquire some sort of reference data, e.g. by known length measurements. From other datasets, we saw that VIF often points towards radial-symmetric parameters being problematic even if the results are accurate. It is unclear whether this behavior was incidental or if it is because of a mathematical instability that generalizes to other geometries. This would have to be investigated further in the future to understand the implications that can be drawn from VIF.

Acknowledgements

This work was funded by the German Federal Foundation for the Environment (DBU, AZ 37885/01-45). Further thanks to the photogrammetry working group at IAPG for valuable feedback and discussion, as well as DENKMAL3D for hosting the experiment in their building.

References

- Agrafiotis, P., Georgopoulos, A., 2015. Camera constant in the case of two media photogrammetry. *Int. Arch. Photogramm. Remote Sens. Spatial Inf. Sci.*, XL-5/W5, 1–6.
- Brown, D. C., 1971. Close-Range Camera Calibration. *Photogrammetric Engineering*, 37(8), 855–866.
- El-Hakim, S. F., 1986. Real-Time Image Metrology with CCD Cameras. *Photogrammetric Engineering & Remote Sensing*, 52(11), 1757–1766.
- Hastedt, H., Luhmann, T., Przybilla, H.-J., Rofallski, R., 2021. Evaluation of Interior Orientation Modelling for Cameras with Aspheric Lenses and Image Pre-Processing with Special

- Emphasis To SfM Reconstruction. *Int. Arch. Photogramm. Remote Sens. Spatial Inf. Sci.*, XLIII-B2-2021, 17–24.
- Kahmen, O., Rofallski, R., Conen, N., Luhmann, T., 2019. On scale definition within calibration of multi-camera systems in multimedia photogrammetry. *Int. Arch. Photogramm. Remote Sens. Spatial Inf. Sci.*, XLII-2/W10, 93–100.
- Kahmen, O., Rofallski, R., Luhmann, T., 2020. Impact of Stereo Camera Calibration to Object Accuracy in Multimedia Photogrammetry. *Remote Sensing*, 12(12), 2057–2087.
- Kotowski, R., 1987. *Zur Berücksichtigung lichtbrechender Flächen im Strahlenbündel: Zugl.: Bonn, Univ., Diss., 1986.* Deutsche Geodätische Kommission bei der Bayerischen Akademie der Wissenschaften Reihe C, 330, Beck, München.
- Kutner, M., Nachtsheim, C., Neter, J., Li, W., 2005. *Applied linear statistical models.* The McGraw-Hill/Irwin series operations and decision sciences, 5th edn, McGraw-Hill Irwin, Boston.
- Luhmann, T., Robson, S., Kyle, S., Boehm, J., 2020. *Close-range photogrammetry and 3D imaging.* 3rd edn, De Gruyter, Berlin, Boston.
- Maas, H.-G., 2015. On the Accuracy Potential in Underwater/Multimedia Photogrammetry. *Sensors (Basel, Switzerland)*, 15(8), 18140–18152.
- Menna, F., Nocerino, E., Remondino, F., 2017. Optical aberrations in underwater photogrammetry with flat and hemispherical dome ports. F. Remondino, M. R. Shortis (eds), *Videometrics, Range Imaging, and Applications XIV*, Proceedings of SPIE, SPIE, Bellingham, Washington, USA.
- Mulsow, C., 2010. A flexible multi-media bundle approach. *Int. Arch. Photogramm. Remote Sens. Spatial Inf. Sci.*, XXXVIII/5, 472–477.
- Nocerino, E., Menna, F., Gruen, F., 2021. Bundle Adjustment with Polynomial Point-To-Camera Distance Dependent Corrections for Underwater Photogrammetry. *Int. Arch. Photogramm. Remote Sens. Spatial Inf. Sci.*, XLIII-B2-2021, 673–679.
- Nocerino, E., Nawaf, M. M., Saccone, M., Ellefi, M. B., Pasquet, J., Royer, J.-P., Drap, P., 2018. Multi-camera system calibration of a low-cost remotely operated vehicle for underwater cave exploration. *Int. Arch. Photogramm. Remote Sens. Spatial Inf. Sci.*, XLII-1, 329–337.
- Rofallski, R., Colson, A., Luhmann, T., 2024. Multimedia Photogrammetry for Automated 3D Monitoring in Archaeological Waterlogged Wood Conservation. *Int. Arch. Photogramm. Remote Sens. Spatial Inf. Sci.*, XLVIII-2-2024, 355–362.
- Rofallski, R., Luhmann, T., 2022. An Efficient Solution to Ray Tracing Problems in Multimedia Photogrammetry for Flat Refractive Interfaces. *PFG*, 37–54.
- Shortis, M., 2019. Camera calibration techniques for accurate measurement underwater. J. Benjamin, W. van Duivenvoorde (eds), *3D recording and interpretation for maritime archaeology*, Coastal Research Library, 31, Springer International Publishing, Cham, 11–27.
- VDI/VDE, 2002. *VDI/VDE 2634 Part 1: Optical 3D measuring systems - Imaging systems with point-by-point probing.* Beuth Verlag GmbH.